Making Comparisons between Abundance Matching and Galaxy Kinematics

Elizabeth Tarantino
Senior Capstone Spring 2016
Advisors: Professor Stacy McGaugh and Dr. Federico Lelli

May 5, 2016

Contents

1 Abstract

In this work, we invoke the method of abundance matching in order to make comparisons between observation and theory. The observations come from the newly formed SPARC catalog which includes 173 accurate rotation curves with Sptizer photometry. This allows a comparison between the kinematics of galaxies and cosmological predictions. Abundance matching uses simulations to form the halo-to-stellar mass relation. This is a correspondence between an observed stellar mass to the theoretical dark matter halo mass. With this expression, we are able to derive values for M_{halo} and R_{vir}. This is then used to plot a Tully-Fisher relation with the theoretical values so a direct comparison to the prediction can be made. We also examine the profiles of two galaxies, UGC 128 and UGC 1230, that are far extended into their dark matter halo. Further, we can take the results from abundance matching and produce a predicted NFW profile for each rotation curve. The profiles shapes tend to overpredict the velocities in the rotation curve but overall abundance matching does a fair job of corresponding well with the average galaxy.

2 Introduction

Evidence for dark matter is found in a variety of different scales in the universe. A mass discrepancy can be seen in the kinematics of nearby galaxies as well as in large scale cosmological simulations. However, different approaches in studying dark matter are rarely compared with each other. The models in an individual subfield tend to be self-consistent, but are they consistent across scales? This work will explore that by examining predictions made from cosmological simulations to the kinematics of nearby galaxies.

Cosmological simulations are great for exploring how we expect the universe to behave with the current paradigm while direct observations of galaxy provide a way to test these predictions. Additionally, often one needs to make comparisons between observation and theory. Cosmological simulations provide a great way of mapping between observed quantities to theoretical ones. This allows direct comparison to what one would expect for a given theory.

Abundance matching is a very successful method of making this transformation that comes out of cosmological simulations (Moster et al. (2013), Guo et al. (2010)). It ties a luminosity or mass function of observed galaxies to a dark matter halo mass function in simulations. The dark matter halo is where the majority of the dark matter in a galaxy resides and is much larger than the galaxy itself. After the functions are tied together, this process then matches the number density of dark matter halos to the galaxy density. This makes a prediction for what dark matter halo mass a galaxy of a given stellar mass will reside in. Also called the halo-to-stellar mass relation, this provides a great way of transferring between theoretical simulation variables to observables. It should be noted, however, that abundance matching is not a physical relation; it is simply a one-to-one correspondence between simulations and observations and will always given an answer for

given data. Nevertheless, abundance matching has also been able to reproduce a variety of observable properties, including the luminosity-velocity relation and clustering of galaxies (Trujillo-Gomez et al. (2011),Kravtsov (2013)).

In conjunction with abundance matching, we also use a sample of galaxies from the newly constructed SPARC catalog. This is a sample of 173 spiral galaxies that contain Spitzer [3.6] μm band data and accurate HI rotation curves from decades of radio interferometry surveys. Rotation curves provide a great way of examining dark matter because kinematics directly measure the total mass enclosed. Radio interferometry data of HI gas is especially useful because it is dynamically cold and follows nearly circular orbits as well as being diffuse and traces the gravitational potential of a galaxy far beyond the stellar components. Figure 1 plots an example rotation curve. In order to isolate the dark matter velocity component, the observed data must be decomposed into its stars, gas, and dark matter. Subtracting out the stars, given from the Spitzer data and a mass-to-light ratio (see Section 2.2.2), and the gas will then give the dark matter component. One can see that the dark matter profile dominates at larger radii while the stellar component is near maximal in the central regions.

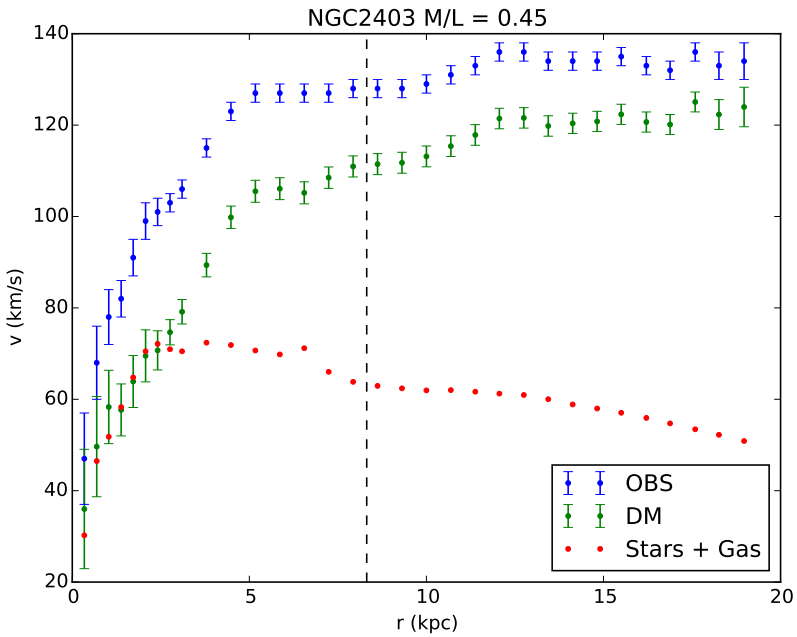

Figure 1: An example rotation curve of NGC 2403

With 173 of these rotation curves, and their corresponding total stellar masses, we can make comparisons between the expected dark matter mass from the kinematics and what

is predicted from abundance matching. Specifically, three projects were carried out in this report. (1) The Tully-Fisher relation, which is a relationship between the stellar mass and velocity of a sample of galaxies, can be transformed into its theoretical values that the relation may be caused by. (2) Two galaxies were found to have highly extended HI profiles in comparison the the radius of the dark matter halo and were examined in detail. (3) An NFW dark matter profile derived from abundance matching was constructed and compared to each rotation curve in the sample.

2.1 Description of Data

The data used in this project is from the SPARC (Spitzer Photometry & Accurate Rotation Curve) catalog. A detailed data write-up of this sample has been submitted by Lelli et al. (2016). This dataset has already been used in publications, such as a study on the small scatter of the Baryonic Tully-Fisher Relation (Lelli et al., 2016). The SPARC database consists of more than 200 high quality HI radio interferometry observations compiled from large surveys and individual studies. Rotation curves in these publications were produced by either fitting a tilted ring model to the HI velocity field or using the position-velocity diagrams along the major axis. Next, the Spitzer archive was searched to find 3.6 μm images of these galaxies in order to create surface brightness profiles and provide an estimate of the stellar mass. 173 objects were discovered with useful [3.6] data and form the full catalog.

The sample includes spiral and irregular disk galaxies that reside in low density environments. They span a large range of mass ($10^8 < \mathrm{M_b/M_\odot} < 10^{11}$), size ($0.3 < \mathrm{R_{eff}/kpc} < 15$), effective surface brightness ($4 < \Sigma_{\mathrm{eff}}/\mathrm{L_\odot pc^{-2}} < 1500$), gas fraction ($0.01 < \mathrm{f_g} < 0.95$), and morphology (S0 to Im). Therefore, this large dataset can be used to make detailed conclusions for a range of galaxies.

2.2 Halo Mass & Radius

2.2.1 Stellar-to-Halo Mass Relation

Abundance matching relies on the relationship between luminosity and stellar mass and helps to connect observations to theory. It is not a physical law; rather it forms a correspondence between the mass function of observed galaxies to halo mass functions in simulations. This creates a stellar-to-halo mass function and provides a conversion between theory and what can be observed. In Moster et al. (2013), the prescription used in this work, the Millennium Simulation and SDSS observations are compared to create a monotonic relationship between M_{halo} and M_*. If the number density of dark matter halos with a given M_{halo} mass matches the number density of observed galaxies with a given M_* then we assume that galaxies of stellar mass M_* reside in dark matter halos of $_{Mhalo}$. This gives a

parameterization of:

$$\frac{M_*}{M_{halo}} = 2N\left[\left(\frac{M_{halo}}{M_0}\right)^{-\alpha} + \left(\frac{M_{halo}}{M_0}\right)^{\beta}\right]^{-1} \tag{1}$$

There are four free parameters in this relation: N is the normalization, M_0 is a characteristic mass, β is the behavior of the relation at low mass ends, and α is the behavior at high mass ends.

2.2.2 Stellar Masses

The mass-to-light ratio (Υ_*) of a given galaxy is usually the largest uncertainty in mass modeling. Population synthesis models tend to find a nearly constant value for Υ_* in the near infrared [3.6] Spitzer band over a range of galaxy types. Near IR is sensitive to older populations with longer lived, redder stars. Younger populations that are bluer and come from recent star formation are not traced well with these near infrared observations. Therefore, the mass to light ratio from near IR [3.6] Spitzer band data appears nearly homogenous despite the current star formation activity of a galaxy. From McGaugh & Schombert (2014), the ideal Υ_* is 0.45 with a scatter of 0.1 dex. It is then simple to estimate the stellar mass from the observed luminosity:

$$M_* = 0.45 L_{[3.6]} \tag{2}$$

This is done for each of the SPARC galaxies. The stellar mass then allows us to make comparisons through abundance matching.

2.2.3 Halo Properties

With this assumed value of stellar mass, we can use the stellar-to-halo mass relation to find the halo mass for each of the sample galaxies from the parameterization in Eq. 1. The halo mass represent the spherical dark matter distribution around each galaxy. We assume that the dark matter halos are virialized, or in equilibrium, and can use the virial theorem to find the radius of the dark matter halo for each galaxy :

$$M_{halo} = \frac{4\pi}{3} R_{vir}^3 \rho_{crit} \Delta \tag{3}$$

The virial radius, R_{vir}, is defined as the total extent of the dark matter halo. Since the edges of a dark matter distribution are difficult to define, the virial radius is defined through an overdensity. R_{vir} is therefore the point at which a galaxy reaches an overdensity, Δ, times the critical density of the universe, $\rho_{crit} = 3H^2/8\pi G$. This over density is set at $\Delta = 200$ in order to be consistent with the work done in abundance matching. With the halo mass found from Equation 1 in the halo-to-stellar mass relation, we can find the viral

radius for each galaxies at this given overdensity. We can then use these physical values to make comparisons to the data directly, forming the connection between cosmology and kinematics of the rotation curves.

The halo masses derived by abundance matching for a given stellar mass are shown in Figure 2. This also gives a representation of the data in SPARC, showing the large stellar mass range and how the halo-to-stellar mass relation behaves with observed stellar masses.

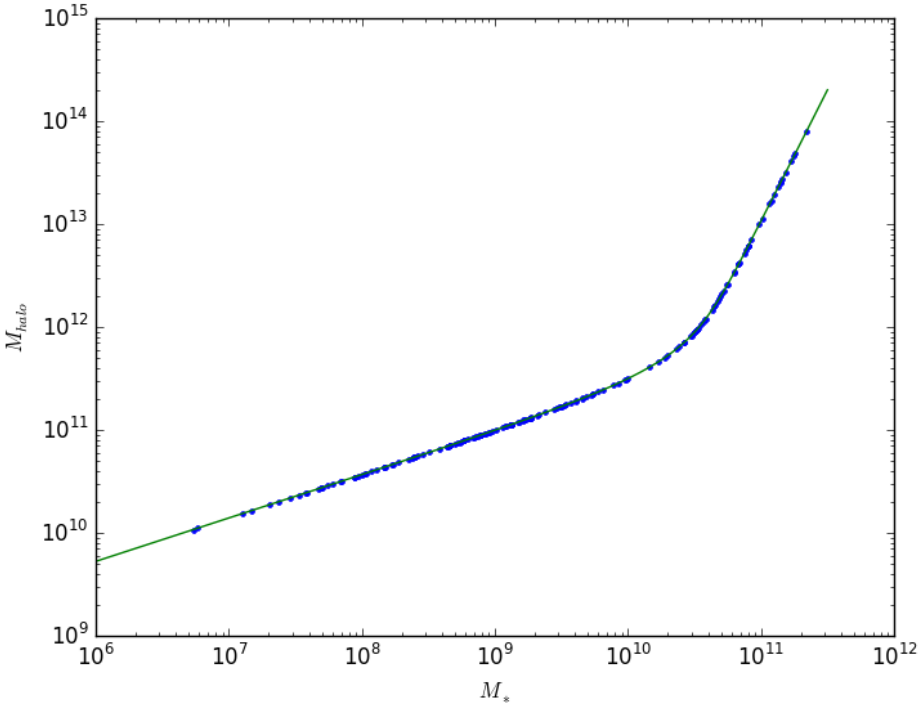

Figure 2: The halo-to-stellar mass relation with the observed stellar masses and the predicted halo masses from the SPARC catalog (blue points). The green line is the halo-to-stellar mass relation used to make the prediction from abundance matching (green line).

3 Dark Matter Halo Tully-Fisher Relation

The Tully-Fisher relation (Tully & Fisher, 1977) is an empirical law for galaxies that relates the total luminosity of a galaxy to a measure of its rotational velocity. These velocities are typically observed through a line width or directly from a rotation curve. The relation itself has become very useful in astronomy as an extragalactic distance indicator. However, the explanation for the Tully-Fisher relation's underlying physical origin and tight correlation

remains unclear. Investigating the nature of the Tully-Fisher relation has potential to inform theories of galaxy formation and dark matter.

There have been many realizations of the Tully-Fisher Relation, for example the Baryonic Tully-Fisher Relation (BTFR), which uses the sum of the gas and stellar mass of a galaxy against its velocity (McGaugh et al., 2000). The BTFR is considered such a fundamental relation, that when the flat velocity of a rotation curve is used, the scatter of the relation is consistent with zero (Lelli et al., 2016).

There are a few explanations for such a strong empirical law, one is relating the total mass to the rotational velocity at the viral radius of a given galaxy. From Equation 3 and with the critical density defined as $\rho_{crit} = 3H^2/8\pi G$, the mass and velocity at the viral radius are related by:

$$M_{halo} = \frac{\Delta}{2G} H_0^2 R_{vir}^3 \tag{4}$$

The circular velocity of a dark matter particle at the virial radius is:

$$V_{vir}^2 = \frac{GM_{halo}}{R_{vir}} \tag{5}$$

This then gives the relationship between halo mass and the "virial velocity":

$$M_{halo} = (\Delta/2)^{-1/2}(GH_0)V_{vir}^3 \tag{6}$$

Removing the constants reveals the proportionality commonly found in the Tully-Fisher relation with a power law slope of 3:

$$M_{halo} \propto V_{vir}^3 \tag{7}$$

However, the halo mass and viral velocity are not directly observable quantities in galaxies. In past work (McGaugh, 2012), the halo mass and virial velocity have been related through the baryon and disk fractions of given galaxies. These values are used to map from the above scaling relation back to the Tully-Fisher relation. However, it is possible with abundance matching to map observable quantities to the theoretical ones, making a prediction. The object of this work therefore is to use the halo mass found from abundance matching to form a type of Tully-Fisher relation derived from the dark halo mass. Instead of using the baryonic mass, this approach will use M_{halo} and a value inferred from the virial velocity.

3.1 Methods

Historically, the velocities chosen for use in the Tully-Fisher have varied depending on the author and approach. When given a full rotation curve, there are a number of velocities to choose from; which one is the ideal? For example, velocities at a given photometric radius,

the effective radius of the galaxy, the point at which the baryons reach peak velocity, or the velocity along the flat part of the rotation curve have all been used in different studies. This last value, V_{flat}, tends to minimize the scatter of the Baryonic Tully-Fisher relation the most (Lelli et al., 2016).

This work is focused on measuring a value related to virial velocity. Because baryons do not go as far out as the virial radius does, we cannot measure the velocity at R_{vir}. Instead, we create a proxy within the limits of the data we have by measuring at a fraction of the virial radius. Figure 3 shows how distributed the galaxies in the SPARC catalog are compared to their virial radii. This represents the extent of a galaxy's baryons in its halo by dividing the last measured point and the virial radius given from abundance matching. By examining the plot, we gain a sense of what fraction or percent would be a good proxy to measure the velocity for the virial radius. We choose 7% R_{vir}, which minimizes the amount of galaxies that would be removed from the analysis while also considering the large spread in virial radii in the sample. Further, the scatter in the Tully-Fisher relation was minimized at this point when compared to 5% or 10%.

3.2 Results

Now that a method to find a proxy for the virial velocity is found, it can be used to form a dark matter halo Tully-Fisher relation. Figure 1 show a dotted line that represents the $7\%R_{vir}$ radii. The velocity of the dark matter closest to this point is then the velocity used for the Tully-Fisher relation. Taking the M_{halo} results from the stellar-to-halo mass relation gives a mass. Instead of plotting a typical M_{bary} vs. V_{flat}, this relation plots M_{halo} vs. Vdm at $7\%R_{vir}$. By transforming the observational values into theoretical ones, gives us the ability to directly compare with the theoretical predictions.

Figure 4 shows this M_{halo} vs. V_{dm} at $7\%R_{vir}$ plotted in log space for the SPARC galaxies that had velocity data at $7\%R_{vir}$. These data were then fitted with a linear regression (solid black line) and had a slope of 3.25 with a scatter of 0.26 dex. The magenta line is directly plotting the predicted relationship between the velocity and halo mass at the virial radius, given in Equation 6. The green line uses the dark matter profile of a galaxy, called the NFW profile (see Section 5 for more information), in order to predict what the velocity will be at $7\%R_{vir}$. The magenta line has a slope of 3 and the green line has a slope of 3.48.

3.3 Discussion

This dark matter halo Tully-Fisher relation behaves similarly to the traditional Baryonic Tully-Fisher relation and achieves a similar slope and scatter. For example, the Baryonic Tully-Fisher Relation values found in Lelli et al. (2016) had a slope of 3.75 and a scatter of 0.11 dex. The scatter is much lower in this case, but when combined with a 0.15 built in scatter for abundance matching, the extrapolated expected scatter is 0.19 dex. This scatter is still smaller than what is observed, but this work used the full sample of galaxies

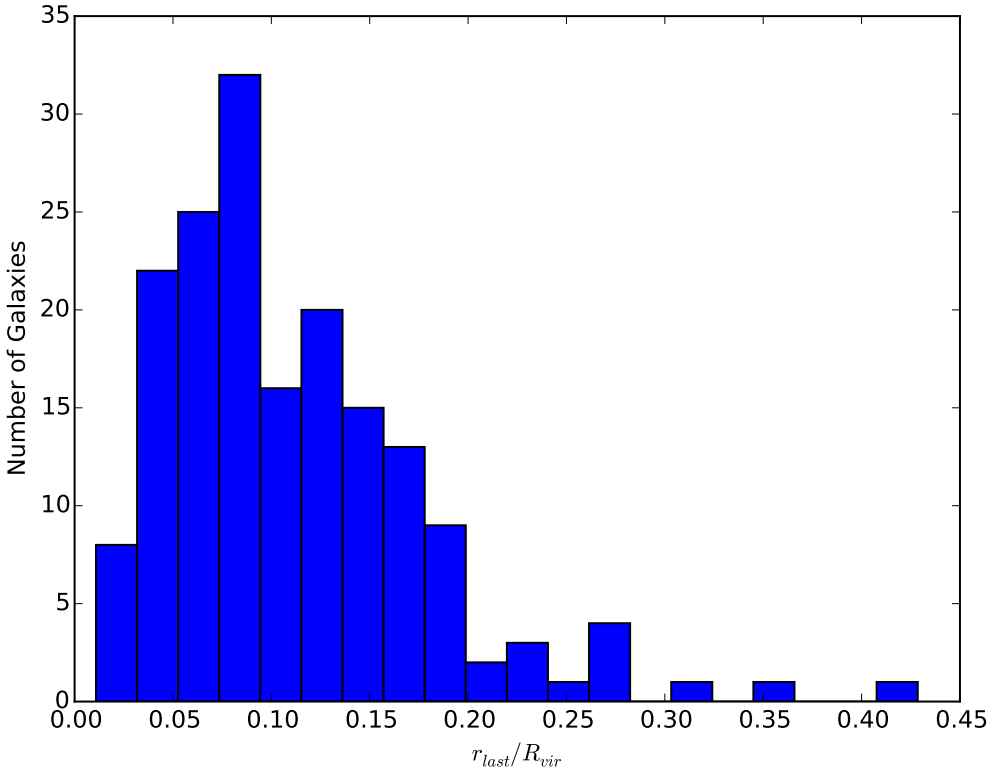

Figure 3: The extent of the baryons in a dark matter halo. Represented by the radius of the last measured point divided by the given galaxies virial radius.

while Lelli et al. (2016) removed interacting and starbursting galaxies.

Further, one may think that the M_{halo} vs. V_{dm} at $7\%R_{vir}$ should not differ if M_* was plotted instead of M_{halo}. Since the halo mass is derived from the stellar mass, they should be approximately the same. However, when this is done, the scatter given from the M_* relation is about 0.1 dex greater than the M_{halo}. This implies that there is something fundamental that comes out of abundance matching that makes the M_{halo} relation have less scatter.

What differs in this work is the predicted Tully-Fisher relation does not contain an offset from the data. In past work, the offset was attributed to the cosmic baryon fraction, f_b, and the disk fraction, f_d. Since M_{bary} was used, a transformation between the halo mass was necessary to compare to theortical predictions:

$$M_{bary} = f_d f_b M_{halo} \tag{8}$$

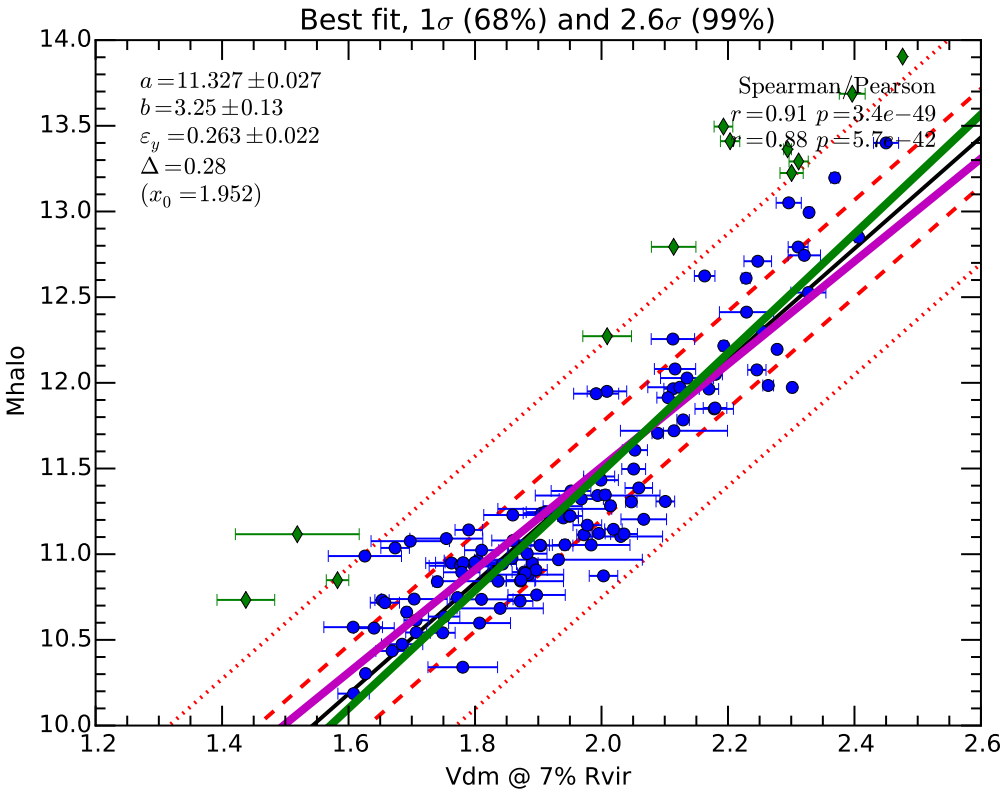

Figure 4: Log-Log plot of the dark matter halo Tully-Fisher relation. Black line is the linear fit. Magenta line is the predicted relation between velocity and halo mass at the virial radius. Green line is the prediction at the observed $7\%R_{vir}$.

The constants f_b and f_d represents the fraction of baryons that can condense down to form a given galaxy. It represents the baryonic physics involved in galaxy formation by describing the transfer from a halo mass to its eventual stellar mass. Abundance matching removes the necessity of this transformation because, by construction, it matches dark matter halos to observed galaxies. Therefore, it has the same normalization as the data. The slopes do not agree with either theoretical prediction, however. This implies that the physics involved in galaxy formation may also effect the slope of the Tully-Fisher relation, not just the normalization. Nevertheless, this work provides a new way of examining the Tully-Fisher relation that translates the data into theoretical values instead of mapping the theoretical predictions into observables.

4 Extended Disks of LSBGs

Low surface brightness galaxies (LSBGs) are very dim objects where the surface brightness, or the magnitude per unit area, is much lower than that of normal, spiral galaxies. They are dominated by neutral HI gas and their stars are spread out a lot thinner than typical galaxies. Low surface brightness galaxies also tend to be more dark matter dominated than their high surface brightness counterparts (McGaugh & de Blok, 1998). The SPARC sample contains a larger proportion of low surface brightness galaxies than other samples, especially because it was constructed based on kinematic surveys of HI gas.

In the typical model of galaxy formation, dark matter halos form by hierarchical accretion and then virialize. Baryons cool and condense towards the very center of these dark matter halos, forming a galaxy. This means that the halos galaxies form inside of are usually much larger than the galaxy itself. Historically, flat rotation curves were the first accepted observational evidence of dark matter. We could then infer the large dark matter halos and, motivated by galaxy formation, were interested in how far the halos extend. Abundance matching says that M_{halo} depends only on M_*, so LSBGs with a large radius for their M_* must extend relatively far into their dark matter halos.

4.1 Methods

As mentioned in Section 3.1, Figure 3 represents how extended the sample of galaxies are in their dark matter halos. Most of the galaxies are clustered around the 7% mark, but there is a wide spread. However, the most interesting aspect are the three galaxies that appear to extend far into their dark matter halos. These galaxies are UGC 128, UGC 1230, and NGC 289. After closer inspection, NGC 289 has a very uncertain distance and is excluded from analysis. UGC 128 and UGC 1230, on the other hand, are very extended LSBGs and warrant further investigation.

4.2 Results

The rotation curves of UGC 128 and UGC 1230 can show how extended they are in radius and velocity while an image of these galaxies gives a sense of the spread in stars. Figure 5 shows these plots for UGC 128 and Figure 6 for UGC 1230. The dashed line represents the 7% line used for the Tully-Fisher work in Section 3, but gives an idea of how extended these galaxies are in the halo.

They are both low surface brightness galaxies, with the effective surface brightness for UGC 128: $\Sigma_{eff} = 20 \mathrm{L}_\odot \mathrm{pc}^{-2}$ and UGC 1230: $\Sigma_{eff} = 29 \mathrm{L}_\odot \mathrm{pc}^{-2}$. They are also gas dominated galaxies, with $f_g = 0.65$ for UGC 128 and $f_g = 0.71$ for UGC 1230. UGC 128 extends 43% into its halo while UGC 1230 extends 32% into its halo relative to R_{vir}.

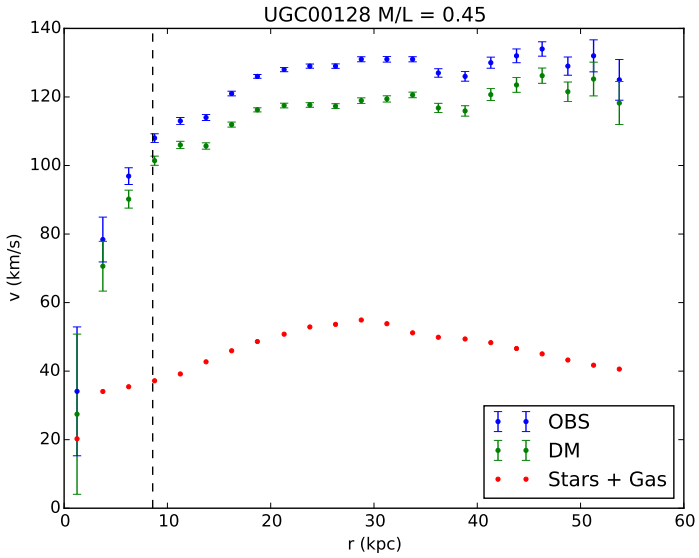

(a) Rotation curve from SPARC

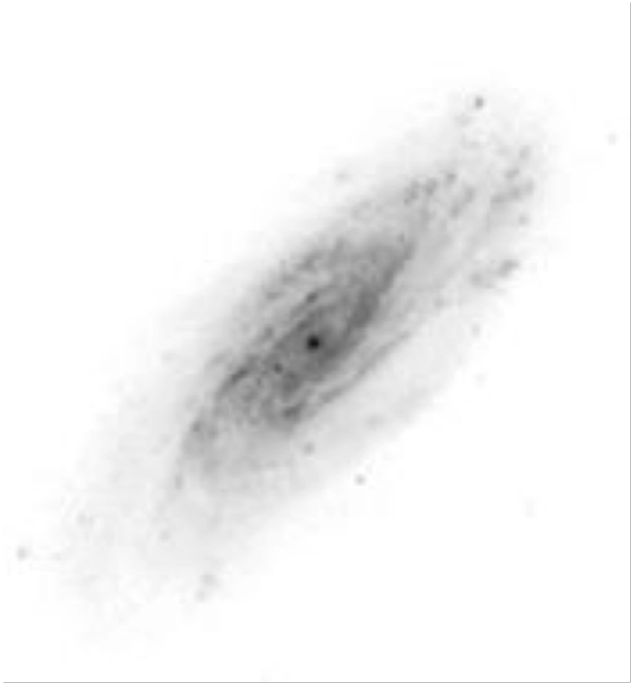

(b) V band image taken from Schombert et al. (2011)

Figure 5: UGC 128

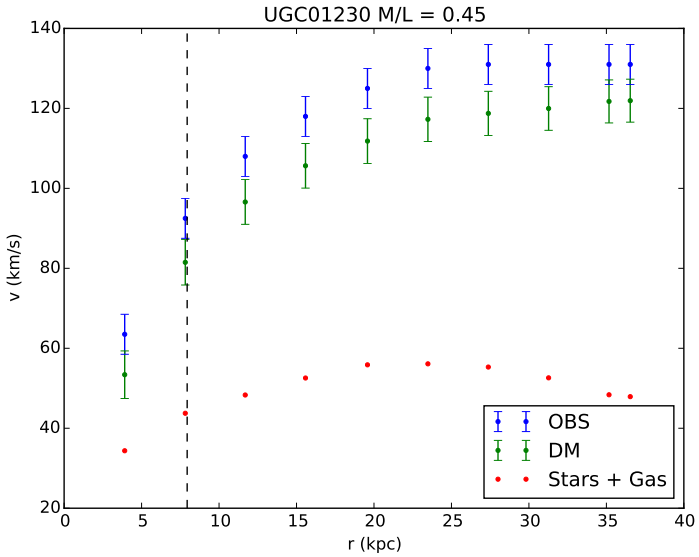

(a) Rotation curve from SPARC

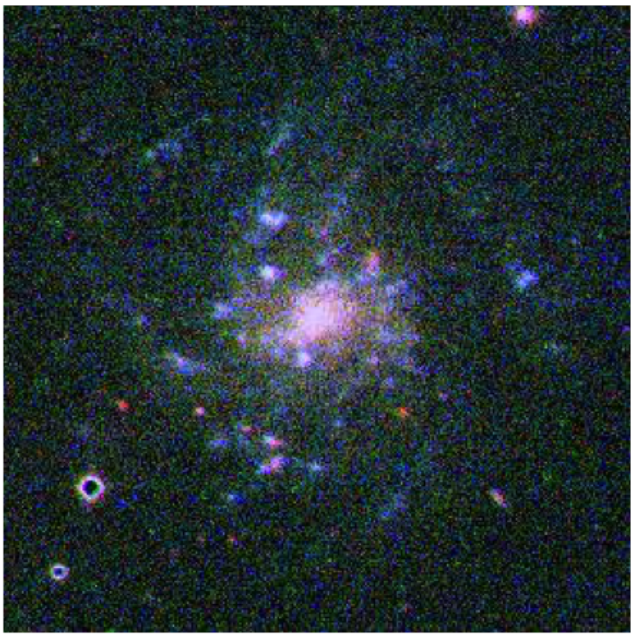

(b) UBVHa composite image taken from McGaugh & Bothun (1994)

Figure 6: UGC 1230

We also calculated the dynamical mass at the last point for each of these galaxies to examine the amount of matter contained in what we can observe from the disk. The dynamical mass is defined as:

$$M_{dyn} = \frac{v^2 r}{G} \tag{9}$$

and the results for UGC 128 and UGC 1230 are shown in Figure 7.

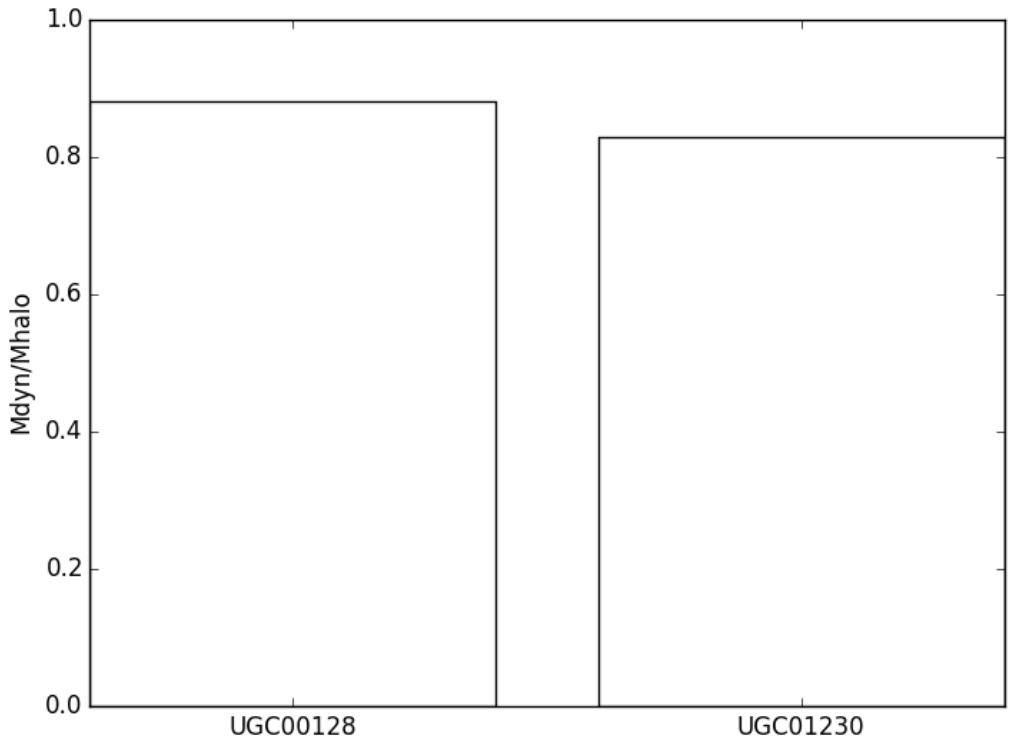

Figure 7: Percentage of total mass contained within the observed rotation curve relative to the halo mass.

4.3 Discussion

There are two basic possibilities for these low surface brightness extended disks. The first is the presumption that these galaxies are actually this extended into their halos. Perhaps in the formation of LSBGs, the baryons become more spread out into the halo itself.

This would follow from the current model of galaxy formation which conserves angular momentum of the spin of the dark matter halo. A low surface brightness galaxy has a much larger scale length compared to regular spiral galaxies with the same mass. However, the same mass implies that the physics in galaxy formation, including conservation of angular momentum, will stay the same. This implies that LSBGs should be more extended into their disks because they have equivalent halo masses but with much larger scale lenghts. However, Figure 7 shows that the observed portions of these galaxies contain over 80% of the total mass. Even considering the large scale lengths of LSBGs, it is unlikely that the rest of the unobserved dark matter halo only makes up 20% of the total mass.

Another possibility is that the abundance matching process has failed for these two galaxies. Abundance matching is not a physical relation, instead it provides a correspondence between observed galaxies to dark matter halos in simulations. Because it's non-physical, the assumptions in abundance matching are especially important when applying it to a sample of galaxies that may be different than the observed galaxies. In this case, abundance matching only takes into account the stellar mass, not the gas mass. UGC 128 and UGC 1230 are gas dominated systems. Therefore, abundance matching may be under predicting the halo mass by not considering the full baryonic content of these galaxies. Further, Moster et al. (2013) uses Sloan Digital Sky Survey data, which does not have many low surface brightness galaxies in its sample. There is consequently extrapolation performed with the galaxies in the SPARC sample since they are unlike those used in the construction of abundance matching. Nevertheless, abundance matching has been very successful in predicting large scale features in galaxies and other LSGBs in this sample do not exhibit the same behavior as UGC 128 and UGC 1230.

Regardless, further investigation of the total sample's agreement to the halo mass calculated via abundance matching must be made to evaluate abundance matching through kinematics.

5 Predicted NFW Profiles

The NFW profile Navarro et al. (1997) is often used to predict the dark matter profile in galaxies. However, it is derived from simulation work of clustering of galaxies, not rotation curves or dark matter profiles from galaxies themselves. It has long been shown that the NFW profile incorrectly predicts the shape of the rotation curve (McGaugh et al. (2007), Moore (1994), de Blok et al. (2001)). Nevertheless, they can still be used to compare the overall total value of the halo mass as a test for abundance matching.

5.1 Methods

The NFW profile's rotation curve parameterization is as follows:

$$V(R) = V_{200}\sqrt{\frac{\ln(1+cx) - \frac{cx}{1+cx}}{x[\ln(1+c) - \frac{c}{1+c}]}} \tag{10}$$

where $x = r/R_{200}$, $c = R_{200}/r_s$, the concentration, and $V_{200} = 10cr_sH_0$. We have values of R_{200}, or the virial radius, for all of our galaxies so we only need to find the concentration to construct NFW profiles for each galaxy. Fortunately, there is the mass concentration relation which describes the relationship between the halo mass of a galaxy and the concentration of the NFW profile. Using the information we have from abundance matching, and the mass concentration relation parameterization from Dutton & Macciò (2014), we can now construct NFW profiles for each galaxy.

5.2 Results

The rotation curve and the NFW profile for three sample galaxies are given in Figure 7, representing an undershoot, overshoot, and a good match. The band represents the 0.15 dex built in scatter in the abundance matching relation. It should be emphasized that the predicted NFW profile is not a fit, but merely the reproduced profile given abundance matching and the mass concentration relation.

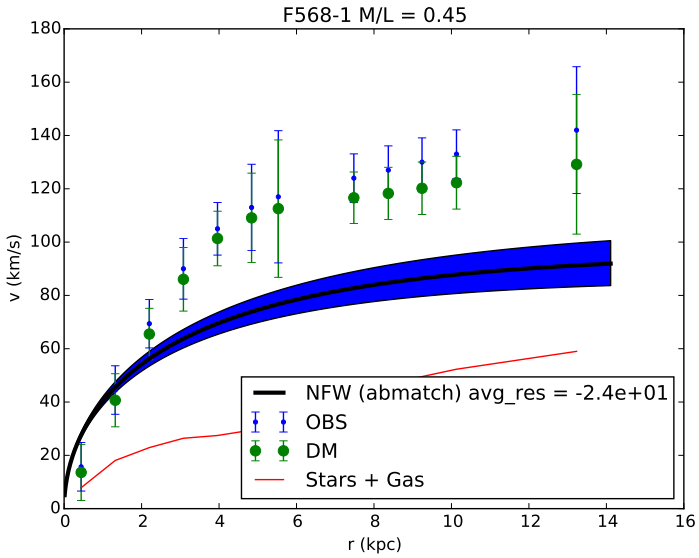

(a) F568-1: Undershoot

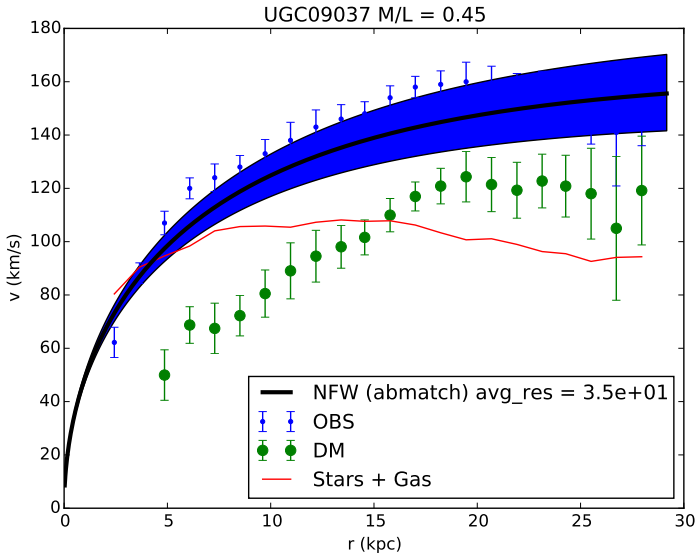

(b) UGC 9037: Overshoot

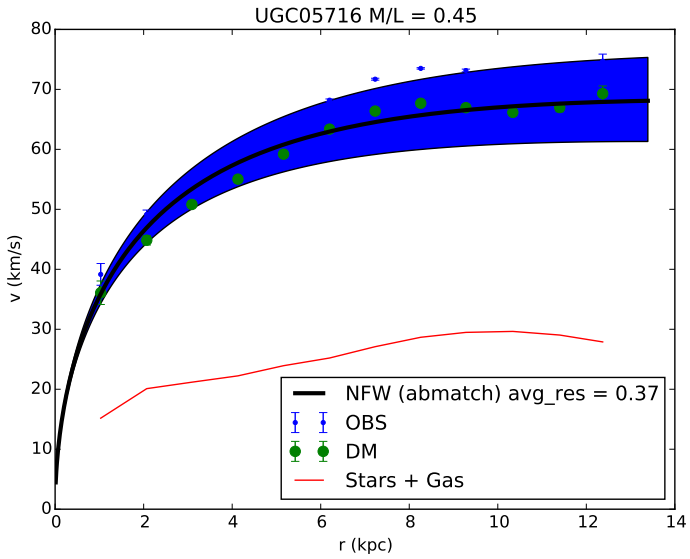

(c) UGC 5716: Good match

Figure 7: Predicted NFW profiles for example galaxies in the SPARC catalog.

5.3 Discussion

It is difficult to analyze how well the NFW profile predicts the overall properties of the rotation curve because of the known discrepancies between the shape of the NFW profile and the shape of observed rotation curves. However, the dynamical mass at the last point is somewhat independent of shape and can provide an adequate measure of how well abundance matching, in tandem with an NFW profile, compares to the direct measure of the mass through kinematics. Figure 8 plots the dynamical mass given from Equation 9 and the mass calculated from the NFW profile at that point for each galaxy. The black line represents a one-to-one correspondence.

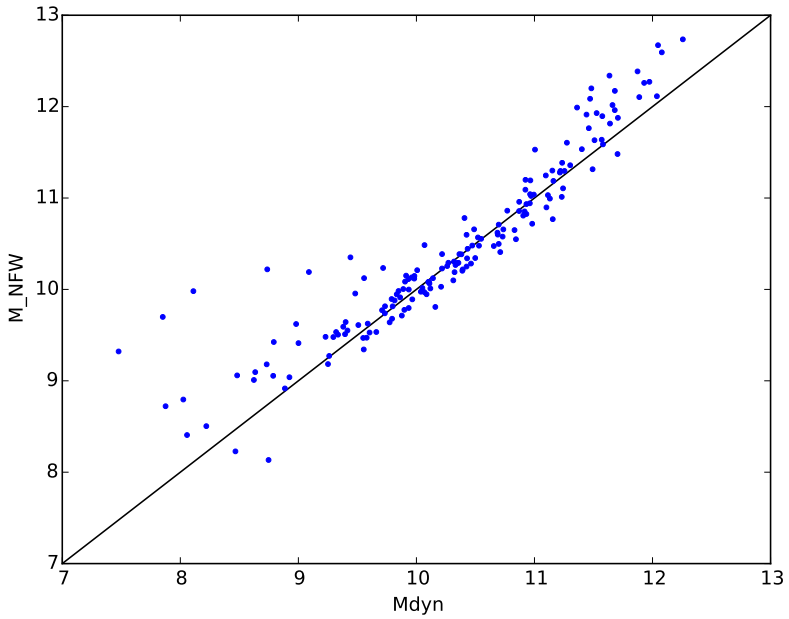

Figure 8

It appears that the abundance matching NFW profiles, on average, tend to predict the dynamical mass relatively well. At the lower and higher mass ends they tend to over predict the dynamical mass. Additionally, there is no relation of surface brightness or gas fraction on the discrepancy between the dynamical mass as measured and calculated via NFW profile. This implies that UGC 128 and UGC 1230's extended behavior may not be due to the high gas fraction or low surface brightness of these objects. Instead, it likely is due to the scale length of these galaxies. Nevertheless, it is interesting to directly examine the NFW profiles for these galaxies and see how they underpredict.

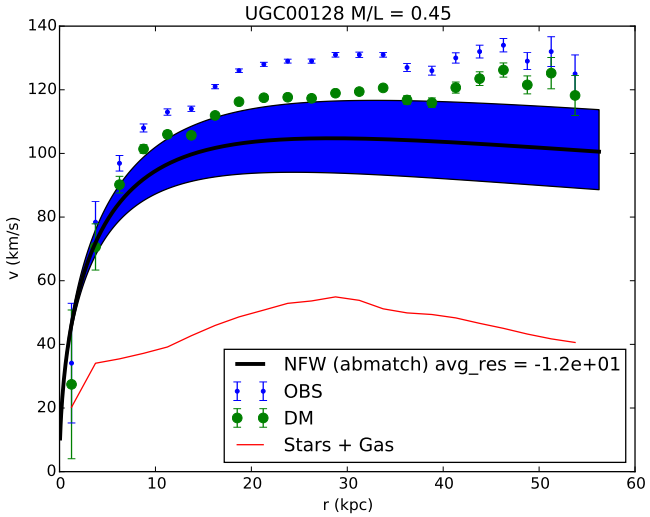

(a) UGC 128

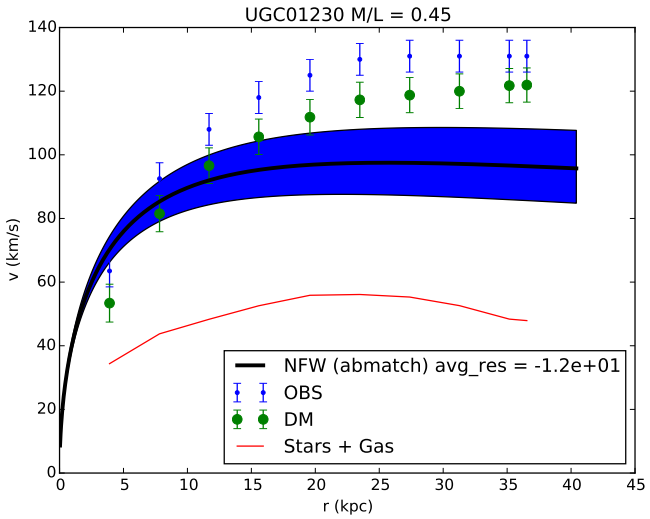

(b) UGC 1230

Figure 9: Predicted NFW profiles

Figure 9 shows the predicted NFW profile for UGC 128 and UGC 1230. One can see that the NFW profile is clearly an undershoot for both galaxies. The profile even appears to be decreasing in velocity for UGC 128 while the observed dark matter velocity stays flat. This shows that there is a clear mass discrepancy from the predicted NFW profile

and what is observed, implying that the mass estimate for the halo is too small for these galaxies to produce a profile that agrees with data. Further, the decreasing NFW profile means that the distribution of the dark matter in low surface brightness galaxies may be more extended than the NFW profile predicts.

On large scales, abundance matching does an adequate job at predicted the masses of observed galaxies. The predicted NFW profile's shape is wrong for most galaxies, but that is likely an effect of the profile, not abundance matching itself. However, UGC 128 and UGC 1230 appear to have a discrepancy between abundance matching and kinematics unlike the other galaxies in the sample.

6 Summary and Conclusions

The goal of this capstone was to make comparisons between cosmological simulations and kinematics of galaxies using abundance matching. Three separate projects were carried out, including the dark matter halo Tully-Fisher relation, examining the extended disks of LSBGs, and comparing predicted NFW profiles to rotation curve data. The Tully-Fisher work yielded a new way of looking at the Tully-Fisher relation that attempts to directly plot the theoretical quantities that derive the relation. There was no offset present in other work as compared to this work because the baryonic physics was contained in the abundance matching. However, the slopes given from theoretical predictions did not match what was observed. This implies that galaxy formation may not present just an offset to the relation but also may change the slope.

The other two projects involved looking at the distribution of dark matter in each galaxy. There were two galaxies, UGC 128 and UGC 1230, that were extensively examined because they had HI profiles that stretched far into their dark matter halo. This means that the parts of the galaxy that were observable contained most of the matter instead of the matter distributing in the unobserved outer parts of the halo. Each galaxy was then examined by constructing an NFW profile predicted by the values derived from abundance matching. The shape of the profile was not well matched by observations, but that is likely due to the NFW profile and not abundance matching. However, the overall mass tended to agree well with kinematics. UGC 128 and UGC 1230 had profiles that were beginning to fall off and likely have a larger or more extended halo mass than what is predicted via abundance matching. In conclusion, we were able to make various comparisons between the observations and theory while also examining peculiarities of individual galaxies.

I would like to thank Professor Stacy McGaugh for his constant support and encouragement. Also thanks to Dr. Federico Lelli for help working with the SPARC data and helpful discussions. We also thank Michele Cappellari for providing LTS LINEFIT. This work was made possible through the support of a grant from the John Templeton Foundation.

References

de Blok, W. J. G., McGaugh, S. S., Bosma, A., & Rubin, V. C. 2001, ApJL, 552, L23

Dutton, A. A., & Macciò, A. V. 2014, MNRAS, 441, 3359

Guo, Q., White, S., Li, C., & Boylan-Kolchin, M. 2010, MNRAS, 404, 1111

Kravtsov, A. V. 2013, ApJL, 764, L31

Lelli, F., McGaugh, S. S., & Schombert, J. M. 2016, ApJL, 816, L14

McGaugh, S. S. 2012, AJ, 143, 40

McGaugh, S. S., & Bothun, G. D. 1994, AJ, 107, 530

McGaugh, S. S., & de Blok, W. J. G. 1998, ApJ, 499, 41

McGaugh, S. S., de Blok, W. J. G., Schombert, J. M., Kuzio de Naray, R., & Kim, J. H. 2007, ApJ, 659, 149

McGaugh, S. S., & Schombert, J. M. 2014, AJ, 148, 77

McGaugh, S. S., Schombert, J. M., Bothun, G. D., & de Blok, W. J. G. 2000, ApJL, 533, L99

Moore, B. 1994, Nature, 370, 629

Moster, B. P., Naab, T., & White, S. D. M. 2013, MNRAS, 428, 3121

Navarro, J. F., Frenk, C. S., & White, S. D. M. 1997, ApJ, 490, 493

Schombert, J., Maciel, T., & McGaugh, S. 2011, Advances in Astronomy, 2011, 143698

Trujillo-Gomez, S., Klypin, A., Primack, J., & Romanowsky, A. J. 2011, ApJ, 742, 16

Tully, R. B., & Fisher, J. R. 1977, AAP, 54, 661